Author Manuscript

Author Manuscript

Author Manuscript

Author Manuscript

HHS Public Access

Author manuscript

Lab Chip. Author manuscript; available in PMC 2020 January 21.

Published in final edited form as:

Lab Chip. 2019 July 21; 19(14): 2404–2414. doi:10.1039/c9lc00340a.

Open source acoustofluidics†

Hunter Bachman[a], **Hai Fu**[a,b], **Po-Hsun Huang**[a], **Zhenhua Tian**[a], **Jonah Embry-Seckler**[a], **Joseph Rufo**[a], **Zhemiao Xie**[a], **Jessica H. Hartman**[c], **Shuaiguo Zhao**[a], **Shujie Yang**[a], **Joel N. Meyer**[c], **Tony Jun Huang**[a]

[a]Department of Mechanical Engineering and Material Science, Duke University, Durham, NC 27708, USA.

[b]Department of Fluid Control and Automation, Harbin Institute of Technology, Harbin, Heilongjiang 150001, China

[c]Nicholas School of the Environment, Duke University, Durham, NC 27708, USA

Abstract

Over the past several decades, a litany of acoustofluidic devices have been developed which purport to have significant advantages over traditional benchtop analytical tools. These acoustofluidic devices are frequently labeled as “labs-on-chips”; however, many do an insufficient job of limiting their dependence on the lab. Often, acoustofluidic devices still require skilled operators and complex external equipment. In an effort to address these shortcomings, we developed a low-cost, expandable, and multifunctional system for controlling acoustofluidic devices in the audible to low ultrasonic frequency range (31 Hz to 65 kHz). The system was designed around the readily available Arduino prototyping platform because of its user-friendly coding environment and expansive network of open source material; these factors enabled us to create a system capable of generating high voltage oscillatory signals and controlling microscale flows in acoustofluidic devices. Utilizing the established open source system, we achieved a series of acoustofluidic applications involving the manipulation of fluids and biological objects in a portable fashion. In particular, we used our open source acoustofluidic devices to achieve active rotation of cells and microorganisms, and operation of an acoustofluidic mixing device which has previously shown potential for viscous sample preparation, in a portable fashion. Additionally, using low frequency flexural waves and our portable system, we achieved acoustofluidic separation of particles based on size. It is our hope that the open source platform presented here can pave the way for future acoustofluidic devices to be used at the point-of-care, as well as simplify the operation of these devices to enable resource limited users to leverage the benefits of acoustofluidics in their work.

†Electronic supplementary information (ESI) available. See DOI: 10.1039/c9lc00340a

tony.huang@duke.edu; Tel: +1 919 684 5728.

Author contributions

Conceptualization, H. B., P. H. H., and T. J. H.; funding acquisition, J. H. H., J. N. M., and T. J. H.; investigation, H. B., H. F., P. H. H., and J. E. S.; methodology, H. B., H. F., and P. H. H.; project administration, P. H. H., Z. T., and T. J. H.; resources, J. E. S., J. R., Z. X., J. H. H., S. Z., S. Y., J. N. M., and T. J. H.; software, H. B., and H. F., and Z. X.; supervision, J. N. M., and T. J. H.; visualization, H. B., P. H. H., and Z. T.; writing – original draft, H. B.; writing – review & editing, H. B., P. H. H., Z. T., J. R., J. H. H., J. N. M., and T. J. H.

Conflicts of interest

No conflicts to declare.

Author Manuscript Author Manuscript Author Manuscript Author Manuscript

Introduction

Rapid increases in medical costs associated with traditional healthcare solutions have motivated researchers to search for novel solutions to this growing issue. Traditional healthcare procedures require patients to visit medical professionals to get tests completed; these tests are sent to centralized facilities for testing and eventual return to the physician for action. This lengthy and costly process has created an interest in point-of-care (POC) medicine, where patients are able to be evaluated and take direct action at a single location. Microfluidics based POC technology promises to decrease the cost and time associated with medical care, revolutionizing and improving patient treatment and diagnosis.[1–6] Acoustofluidic technologies, which combine acoustics and microfluidics, have demonstrated promising potential for the design and integration of POC technologies.[7–12] Acoustofluidic technologies have the capability of interacting with fluidic environments in a contact-free and precise manner;[13,14] this capability has been leveraged to achieve many useful applications in biology and medicine including sample concentration,[15,16] sample mixing,[17–19] sample delivery,[20] and cell/particle separation.[7,21,22]

While all of these factors make acoustofluidic devices excellent candidates for use at the POC, one of the major draw-backs associated with acoustofluidic devices is the additional equipment needed to operate effectively; commonly, acoustofluidic devices rely on bulky and expensive function generators for signal generation, amplifiers for increasing the signal power, syringe pumps for precise fluid manipulation, and microscopes for microscale imaging.[13,14,17,23,24] Although acoustofluidic devices are presented as simple solutions to complex problems, each of these external systems introduce operational constraints that hinder the use of acoustofluidic technology at the POC, making the technology less approachable to researchers and clinicians who could benefit from it. Some techniques in microfluidics, including paper[25,26] or capillary force driven[27–29] designs, circumvent the need for some of this equipment. However, these techniques sacrifice the ability to actively control the fluid environment and do not offer the same level of dynamic interaction as some of their microfluidic and acoustofluidic counterparts. Therefore, in order to achieve the benefits of acoustofluidic technology while maintaining POC potential, and open the door to wide-spread adoption of the technology, tools that can control these devices in a user friendly and portable manner must be developed.

In this article, we present an open source technology based control system for use with many acoustofluidic tools. The system is based on the readily available Arduino prototyping platform, and allows for the integration of the key components for acoustofluidic device operation. We use this open source acoustofluidic system to operate several flexural wave based devices,[7,21] achieving functions including rotation of cells and microorganisms, and operation of a device which has the potential to achieve viscous sample liquefaction, in a portable manner. Additionally, using an open source syringe pump design, we also achieved size-based portable particle separation, using low-frequency flexural waves. This is the first time that size based separation has been achieved using the low frequency, sharp-edge based system, and provides future potential for designing a total analysis system based on the flexural wave dependent designs. Microscopic imaging functionality was also demonstrated

Author Manuscript Author Manuscript Author Manuscript Author Manuscript

with the use of low-cost optical components and an Arduino compatible camera. Even with all of the components, the system could easily fit into a backpack, and weighs less than 5 lbs. This makes the entire system easily transportable, capable of being brought to the POC without difficulty. Table 1 provides a summary of the device performances achieved by the power control portion, as well as the add-ons.

We chose to design our acoustofluidic system around the Arduino platform because of its large network of open source examples, readily available components, and ability to easily expand the system for many different needs.[30–32] The system is compatible with either wall or battery powered supplies, making it an excellent candidate for POC applications. The cell/microorganism rotation demonstrated in this work has the potential to directly benefit research efforts such as drug discovery, where rotation-based 3D imaging allows researchers to gather a greater amount of information from their samples using a conventional microscope.[24,33] With regards to sample preparation, typically the high viscosity of some samples necessitates lengthy and complex processing steps to unlock their diagnostic potential. Our bio-contained acoustofluidic mixing chip demonstrated within has previously shown the potential to handle these complex samples and could be integrated with additional microfluidic analysis techniques to bring a low-cost diagnostic tool to resource-limited settings.[17] Finally, the unique flexural wave-based particle separation technique uses solid oscillating sharp-edges on the channel wall to trap particles based on their size. This acoustofluidic device could be adapted to capture particles of interest or purify biological samples for downstream testing.[21,34] With its open source and expandable nature, and its ever growing portfolio of tools, the open source acoustofluidic system presented here can help bring the field of acoustofluidics to real-world applications. Additionally, the methods and applications demonstrated have far reaching implications for research areas outside of simple acoustofluidic manipulation, including POC microfluidics and biomedical research as a whole. We believe that the work presented here serves to demonstrate and showcase the potentially simple and effective nature of our acoustofluidic technology, making the platform more approachable to a wide variety of potential users.

Control system and acoustofluidic device design

Design, integration, and control of the open source platform

When replacing the bulky equipment needed to operate acoustofluidic devices, the primary concern is delivering the requisite input signal to the acoustic transducer. To accomplish this task, we used an Arduino UNO (part no. A000066, Arduino) prototyping board to control a high voltage signal that was passed to the transducer. A dual full-bridge motor driver control board (L298N2A, TronixLabs) interfaced with both the low voltage Arduino platform and the high voltage power supply and acted as an intermediate between them. Fig. 1a provides a photograph of these critical elements; from left to right, there is the Arduino Uno (this could be replaced with any comparable prototyping board which offers similar functionality), a solderless breadboard for simple prototyping (which could be replaced with a printed circuit board after finalizing your system), and the motor driver to pass a high voltage signal to the acoustic transducer.

Author Manuscript Author Manuscript Author Manuscript Author Manuscript

The Arduino must be supplied with a voltage between 5 and 12 volts, and the motor driver should be supplied with a higher voltage DC source that is at the amplitude you wish to supply your device with. The L289N microchip is limited to 50 V for the high voltage signal. Since the transducer requires an alternating signal to generate its oscillations, the high voltage DC source must be converted into an oscillatory signal using the Arduino board. Fig. 1b provides a schematic to describe the process through which the high voltage DC signal is converted to an alternating signal using the system. Simply, the low voltage Arduino board is used to produce an oscillatory ON/OFF signal which opens and closes the high voltage circuit between the motor driver and the transducer. That is, a 5 volt signal leaves the Arduino and enters the motor driver. This signal causes the motor driver to close the circuit connecting the high voltage DC supply to the transducer. The Arduino signal is then switched off, causing the motor driver to open the circuit between the transducer and the supply, removing the voltage from the transducer element. Therefore, if a control signal from the Arduino is sent to the motor driver at a given frequency, the high voltage alternating signal will be applied to the transducer at the same frequency. This alternating frequency is the frequency that the transducer receives and is translated into oscillatory motion necessary to operate various acoustofluidic devices. As such, the user only needs to specify the frequency of the desired signal, and the Arduino will pass that signal into the motor driver to power the transducer. The operator can connect either a wall powered DC supply, or a battery to the high voltage IN lines of the motor driver, allowing for an adaptable system based on the operational setting (see Fig. S1 in the ESI† for oscilloscope images of signals generated from different operational parameters). In order to give the user basic control over the system, we designed the platform with 3 control buttons. Two buttons control the frequency (increasing or decreasing the frequency by a pre-set interval) and a third button turns the signal ON or OFF. An LCD screen displays the current frequency and updates as the user sets their desired value, and an LED indicates whether the system is currently operating. Additional control parameters, such as pulsed operation, could either be coded into the program or integrated *via* additional control buttons. In an effort to promote the open source nature and collaboration of this work, the Arduino code used to operate the acoustofluidic device has been included in the ESI.†

It is important to note that using this code and these specific components imposes several limitations on the operational parameters. We have already mentioned that the motor driver imposes a 50 V max on the high voltage input, and the Arduino code used restricts the output frequency to between 30 Hz and 65 kHz. Further discussion of these limitations is included in the ESI.† Additionally, alternative code or components could be used to adjust these limits to the needs of a specific application. For example, many acoustofluidic technologies rely on signals with frequencies approaching and exceeding the MHz range. If desired, researchers could manipulate the Arduino microchip's timers directly and generate signals that extend into the low MHz range; pairing these signal with appropriate circuitry could produce the higher frequency signals needed to expand the range of acoustofluidic devices that can be operated at the POC. Once we verified that the system was functional with these specific parts, we sought to validate the system using a variety of acoustofluidic

†Electronic supplementary information (ESI) available. See DOI: 10.1039/c9lc00340a

Author Manuscript Author Manuscript Author Manuscript Author Manuscript

demonstrations. This involved testing new acoustofluidic devices, as well as verifying the performance of devices we have already created in the lab.

Design and fabrication of acoustofluidic devices

The acoustofluidics devices featured in this paper rely on bulk acoustic wave (BAW) vibrations. The BAW vibrations of a disc style piezoelectric transducer create a flexural wave pattern on the surface of a glass coverslip. These flexural waves are used to excite features within the microfluidic channel; these features provide a pathway for interaction between the vibrations and the fluids and particles within the channel. The two main devices used in this work rely on sharp polydimethylsiloxane (PDMS) protrusions or an air-bubble within the channel to transmit these vibrations. The former devices are termed sharp-edge based acoustofluidic devices, and the latter are referred to as bubble based acoustofluidic devices. In the sharp-edge based acoustofluidic device, low frequency flexural waves (3–6 kHz) excite the tips of the sharp edge protrusions, creating oscillations. These oscillations generate acoustic streaming in the fluid which is leveraged for various applications. We would like to note that these frequencies are within the audible range, and as such generate a noticeable sound when the transducer is activated. The sound level produced during operation can be compared to the level produced by a common cellphone; this noise could be reduced by placing the device in a small enclosure during testing. The bubble based acoustofluidic device relies on higher frequency signals which approach and exceed the audible and ultrasonic boundary (>20 kHz). These vibrations cause the surface of the bubble to oscillate, once again creating acoustic streaming. The application of this fluid interaction will be explored in various experiments throughout this work.

Both of the acoustofluidic device types used in this work were fabricated using similar methods, both relying on soft lithography techniques. The sole difference is that the solid master molds used to create the sharp-edge based devices were created using a deep reactive-ion etching (DRIE) process,[35] whereas the mold for the bubble based devices relied on a basic SU-8 photolithography process.[24] The differences in fabrication requirements arises from the fact that the small feature size in the sharp-edge based system requires a higher aspect ratio that can only be achieved with the DRIE process. Once master molds were fabricated, the PDMS channels were formed by mixing a 10 : 1 ratio of Sylgard 184 silicone elastomer base and curing agent (Dow Corning) and pouring it over the mold. A vacuum chamber was used to remove bubbles from the curing PDMS before it was solidified in an oven for 1 hour at 65 °C. After the point, the individual channels were cut from the mold and had inlets and outlets punched to the appropriate size. The PDMS chips were then bonded to a glass coverslip (CAT. no. 48404–455, VWR) after a brief surface plasma treatment (BD-10AS, ElectroTechnic Products) for 30 s. After bonding, the chips were baked in a 65 °C oven for 24 hours to fully cure. After this final curing, the acoustic transducers (AB2746B-LW100-R, Digi-Key Electronics) were fixed to the glass slide adjacent to the PDMS channel using a 5 minute epoxy (PermaPoxy™ 5 Minute General Purpose, Permatex). Although a cleanroom is needed to fabricate a master mold, once it has been created it can be used to fabricate many PDMS devices; with an extensive curing process at room temperature, and a simplified bonding procedure, these devices can be assembled outside of the cleanroom with minimal external equipment. Fig. 1c and d

Author Manuscript Author Manuscript Author Manuscript Author Manuscript

provides photos of two acoustofluidic devices used during validation, including a sharp edge based acoustofluidic sputum liquefaction chip, and a bubble-based acoustofluidic device for rotational manipulation. Images taken throughout experimentation were captured using an inverted microscope (Nikon) and either a CCD camera or fast camera depending on the frame rate requirements of the experiment.

Results and discussion

Arduino control system powered by an electrical outlet

When first testing the system, it was simplest to design and operate using a wall powered electrical supply. We believed that these power systems, seeing as they are commercially manufactured, would provide a more consistent and workable source for the early stages of development. As such, we conducted our initial testing using wall powered supplies for both the Arduino (low voltage input) and the motor driver (high voltage input). That is, a standard 9 V, 650 mA wall plug was used to power the Arduino, and a variable voltage DC supply was used to provide the high voltage source that would be passed to the acoustic transducer. Using these devices, we were able to produce the alternating high voltage signal that is found in Fig. 1b.

As an initial demonstration of our system, we sought to operate the acoustofluidic, sharp-edge based micromixer and micropump. The micromixer was infused with DI water and fluorescein from a Nemesys syringe pump and the Arduino signal was varied from 3.0 to 4.5 kHz. Fig. 2a provides fluorescent images of the mixing performance with varied input frequencies, and Fig. 2b provides a plot of the mixing index given across the entire range of frequencies tested. The mixing index is defined as the standard deviation of the normalized intensity values across the width of the channel, where 0.0 and 0.5 represent completely mixed and unmixed solutions, respectively. A mixing index of 0.1 is used to define sufficient mixing in the channel. The DC power supply was set to 35 V and the total flow rate from both inlets of the mixer was 10 μL min^{-1}. A characteristic dip in the mixing index was achieved with respect to the frequency domain, indicating the resonance frequency of each device. As usual, subtle differences in the construction and fabrication of each device instils variations into each device's specific frequency response, resulting in the standard deviations shown in the plot. Even though the individual responses of each device vary across the frequency spectrum, certain frequencies are shared across all devices; for this acoustofluidic mixing device, the frequency of 3.6 kHz could be specified as the optimal frequency, and would provide complete mixing across all devices.

A similar procedure was used for the acoustofluidic pumping device, where we varied the frequency supplied by the Arduino signal from 4.0 to 6.0 kHz, while setting the DC power supply to 30 V to obtain Fig. 2c and d. Fig. 2c shows overlaid images tracking two particles moving in the channel when supplied with excitation signals of varied frequency (5.4 kHz and 6.1 kHz). We can see that in a time frame of 288 ms, the particle moving in the pump excited by the 5.4 kHz signal outpaces the 6.1 kHz particle. Viewing the results of the plot in Fig. 2d, we can see the expected resonant response, and note that the peak occurs at 5.4 kHz, where the average flow rate was approximately three times that of the flow rate when the pump was excited by the 6.1 kHz signal (9.56 μL min^{-1} *vs.* 3.11 μL min^{-1}, respectively).

Author Manuscript Author Manuscript Author Manuscript Author Manuscript

The flow rate was determined by tracking the particle velocity using ImageJ software and analyzing videos of the flowing particles. These results are comparable in performance to our previously reported results,[8,20] validating the performance of the system for controlling sharp-edge based devices; that is, these results serve to demonstrate the functionality of the system within the audible range where the sharp-edge chips operate. However, the majority of acoustofluidic devices operate above the audible range, and as such, a successful control platform must be able to function in this region.

For our next investigation, we sought to determine whether or not the system was capable of operating other acoustofluidic devices that function at much higher frequencies than those of sharp-edge based devices; previously developed solutions for portable operation were not able to generate signals above the audible range.[8] For this exploration, we used the acoustofluidic technique of harnessing the vibrations of oscillating bubble surfaces to achieve fluid manipulation.[36] A schematic of the bubble based device used in this experiment can be found in Fig. 3a. Although the strength of vibrations generated within the glass slide and microfluidic system are much lower at these higher frequencies, the vastly lower stiffness of a bubble surface compared to a solid PDMS structure creates stronger streaming with less vibrational input. The vibrations of the bubble surfaces creates acoustic streaming and radiation forces that act on the fluid and particles or organisms within the fluid domain. The acoustic streaming affects local particles through an induced drag force which can be approximated using the equation for Stokes' drag and the velocity of the microstreaming generated by the bubble. These equations are given by:[37]

$$F_{\mathrm{AD}} = 6\pi\mu a_{\mathrm{p}} u_{\mathrm{s}} \tag{1}$$

$$u = \frac{a_b^4}{d^5}\omega\varepsilon^2 \tag{2}$$

where μ, a_{p}, and u_{s} are the dynamic viscosity of the fluid, radius of the particle, and non-oscillatory velocity of the particle relative to the fluid, and the streaming velocity of the particle is dependent upon the radius of the bubble (a_{b}), distance from the bubble (d), angular frequency of the applied signal (ω), and the displacement of the bubble surface (ε). The non-oscillatory velocity relative to the flow can be calculated by taking the difference between the background flow velocity and the streaming velocity given in eqn (2). The acoustic radiation force produced by an oscillating bubble also acts to attract or repel particles based on the following relationship:[37]

$$F_{\mathrm{R}} = \frac{4}{3}\pi a_p^3 \Phi(\rho)\frac{a_b^4}{d^5}\omega^2\varepsilon^2 \tag{3}$$

$$\Phi(\rho) = 3\frac{\left(\rho_{\mathrm{p}} - \rho_{\mathrm{f}}\right)}{2\rho_{\mathrm{p}} + \rho_{\mathrm{f}}} \tag{4}$$

Author Manuscript Author Manuscript Author Manuscript Author Manuscript

where ρ_p and ρ_f represent the density of the particle and the surrounding fluid, respectively. When the density of the particle is greater than that of the fluid, an attractive force is generated, pulling the particles towards the bubble surface. Conversely, a particle density which is less than that of the bulk fluid results in a repulsive force acting on the particle. These are the two primary forces that act on particles and cells within an acoustic streaming velocity field, and it is the balance between these forces which determines how these objects act when the acoustic field is active. All of the objects manipulated in this article have a density greater than the water they are contained in, and so they are attracted to the bubble. As such, it is the balance of this attractive force and the streaming related drag that governs particle motion.

Leveraging the streaming pattern generated in the channel, we were able to use our portable acoustofluidic control platform to rotate an important model organism, the nematode *Caenorhabditis elegans*. Rotation of the worms relied on the out-of-plane streaming generated by the bubble and sketched in Fig. 3b; this view looks at a cross section of the channel, as marked by the red arrows in Fig. 3c. Using this device, *C. elegans* are rotated along their long axis, which was previously reported as advantageous when investigating the internal structures of the worms.[24] Certain features may be obstructed when viewing *C. elegans* from a given angle, and so the ability to rotate the worm for viewing from multiple angles can help researchers unearth hidden, potentially critical data.

In order to ensure that clear images are captured during rotation, *C. elegans* are paralyzed using a 1 mM solution of sodium azide before being injected into the channel; this prevents the worm from moving during image capture and creating unfocused images. Fig. 3c provides a full body view of an approximately 8 day old adult *C. elegans*, as well as a close-up of the proximal posterior gonad captured throughout rotation. In order to rotate the nematode, a signal of 20 V and 19.1 kHz was applied to the bubble based device. As seen in the photos, the worm is smoothly rotated around its entire length. In the initial frame, the oocytes can be seen clearly in the gonad region, before rotating out of sight in the middle frames, and returning in the final frame. Using these oocytes as markers, we can see that one full rotation for this worm took 1.144 s, corresponding to a rotation speed of 52.4 RPM, which was extremely consistent throughout the rotation (see Video S1 in the ESI† for video of the rotation). In another experiment, worms rotated with a 30 V and 18.5 kHz signal were consistently rotated at 227 RPM, much faster than the worm shown in the video, and consistent with the expected increase in velocity from a larger input voltage and larger bubble deflection.

Arduino control system powered with batteries

To this point, we had been operating the system using power supplies that depend on electrical outlets. However, not all POC situations allow for an unlimited supply of electricity, and more portable power solutions need to be devised. In order to address this situation, we developed and modified the Arduino platform for use with a battery power supply system. This system was composed of several rechargeable lithium ion batteries (part no. 1568–1429-ND, Digi-Key Electronics) like those found in most portable electronics wired in series to generate the high voltage source that would be applied to the transducer.

Author Manuscript Author Manuscript Author Manuscript Author Manuscript

Each battery had a rated voltage of 3.7 V, and so six of them were used to obtain at least 22 V (actual voltage ranged up to 25 V due to variations in individual battery performance). Two additional batteries were used to supply the Arduino board with the power it needed. For this power system, it would also be easy to integrate a DC–DC voltage converter with the battery supply to further increase the voltage, or offer dynamic control. For the demonstration of this system, we simply used the batteries in the described configuration.

After validating the signal produced by the battery powered device, we chose to demonstrate the functionality of the system by using the in-plane rotation capabilities of the bubble-based acoustofluidic platform. In the in-plane mode, counter rotating vortices are generated on either side of the bubble when viewed from the top of the device. Fig. 4a provides a schematic of the in-plane streamlines generated by the oscillating bubbles, and Fig. 4b provides a particle tracing for 1 μm red fluorescent particles. Streamlines on the left side of the bubble travel in a counterclockwise direction, whereas the right side experiences clockwise rotation. To take advantage of this streaming, we rotated HeLa cells using this in-plane rotation. Both clockwise and counterclockwise rotation was achieved depending on which side of the bubble the cell was located. In Fig. 4c, a cell on the left of the bubble was rotated with a signal of 20.9 kHz, and the cell on the right side of a bubble (Fig. 4d) was rotated using a signal with a frequency of 21.8 kHz. Fig. 4e and f provide plots of the rotation angle *versus* time for each of the cells. It can be seen that the rotation speeds varied between these two cells/frequencies from 104 RPM to 61.7 RPM, respectively. This is counterintuitive to the idea that the streaming velocity should increase for higher frequency excitation (eqn (2)); although, this inconsistency is a common issue found in resonance based systems. Inconsistencies in bubble shape, size, or location within the device create variations in each of the parameters affecting the streaming and radiation, thus varying the performance. Nonetheless, when an attempt is made to keep parameters the same, generally consistent performance can be achieved. Fig. S1 in the ESI† shows two cells which are being rotated at the same time (meaning the same voltage is applied, and the frequency is the same). Although there is a slight difference in the rotation angle, the cell movements nearly mirror each other. Regardless of this fact, with the proper frequency and amplitude adjustment, the battery powered device would be capable of rotating cells and *C. elegans* at any desired rate or pattern. This cell-based experiment has served to demonstrate the successful transition of the Arduino based platform from wall powered operation to portable, battery powered functionality, even at ultrasonic frequencies. While the battery powered Arduino system significantly increases number of settings that the acoustofluidic devices can be operated in, some devices may still be reliant on additional external equipment for full functionality.

Adaptations and expansions

One of the benefits associated with using an open source platform like the Arduino prototyping system is the availability of commercial components that can be seamlessly integrated into the design. As a critical element in the operation of many acoustofluidic and microfluidic designs, we developed and integrated a portable syringe pump based on a stepper motor.[32] This is a perfect example of the open source nature, owing to the fact that these portable pumping systems have already been proposed and developed for alternative

Author Manuscript Author Manuscript Author Manuscript Author Manuscript

applications. As such, it is up to the researcher to determine how to modify and tailor the plethora of available technologies to suit their needs. The portable syringe pump system that was created to be compatible with our acoustofluidic setup has been included in Fig. 5a. The working principle of the fluid delivery system is that a stepper motor (part no. ROB-09238, SparkFun Electronics) turns a threaded rod which passes through a nut which is affixed to a syringe “sled”. In this configuration, rotating the threaded rod causes the nut/sled system to translate and depress the syringe plunger. A motor shield (part no. 1438, Adafruit) was used as an interface between the 12 V power signal for the motor, and the lower voltage circuitry of the Arduino board. 3D printed parts were used to fabricate a mount for the motor, as well as create the syringe sled and syringe fixture (Fig. 5A). Using the code library associated with the motor shield, we were able to develop our own control code and demonstrate variable flow rate generation across a range of speeds. Fig. 5b provides a plot of the flow rates generated by the portable syringe pump when varying rotational speeds are input. A strong linear correlation ($r^2 = 0.9995$) was achieved, and is expected when turning the threaded rod with a constant pitch. With the 1 mL syringe that we used during the calibration, we were able to achieve a minimum flow rate of 11.2 μL min^{-1} at 1 RPM. Calibrating the device based on the rotational speed also enables users to create an even wider range of flow rates simply by changing the syringe size. That is, since the syringe sled will move at a constant rate based on the motor rotation, a syringe with a wider cross sectional area will inherently eject more fluid when it is depressed the same distance as a smaller syringe. We leveraged this fact to decrease the minimum flow rate to 3.33 μL min^{-1} by using a 250 μL syringe.

Once we had calibrated the pumping system, we used it in conjunction with the Arduino-based acoustofluidic control platform to validate an acoustofluidic design for mixing viscous biological samples, as well as demonstrate, for the first time, sharp-edge acoustofluidic based separation of particles based on size. If the sharp-edge is modelled as a cantilevered beam, then the tip deflection can be shown to be proportional to the length cubed. This means that a significant increase in mixing performance can be achieved with the longer sharp-edge length. This increased streaming is necessary for properly mixing viscous samples such as sputum. The outlet of the chip has a filtration region which serves to remove the unwanted debris from the sample before it leaves the microfluidic channel. We tested this system by mixing fluids at various flow rates (Fig. 5c). With an applied signal of 30 Vpp (from a DC power supply) and 4.8 kHz (regulated by the Arduino system), the acoustofluidic chip was able to mix the DI water and fluorescein at a total flow rate of up to 79 μL min^{-1} before the performance began to suffer. Although this work is preliminary in nature, we hope to create future platforms which integrate this strong mixing performance with downstream analysis techniques for POC testing and diagnosis. It is important to note that the strong mixing performance of this acoustofluidic chip while using DI water and fluorescence is only representative of the potential to achieve viscous sample mixing. In experiments with more viscous fluids, the flow rate of the samples must be reduced to maintain sufficient mixing performance, similar to our previous results.[17]

To achieve sized based separation of particles using the sharp-edge acoustofluidic platform, we leveraged the acoustic streaming and radiation forces generated from their vibration. This technique balances the drag force experienced by a particle in the bulk flow with the

Author Manuscript Author Manuscript Author Manuscript Author Manuscript

radiation force and acoustic streaming related drag force generated by the vibrating surface. Using the syringe pump and 250 μL syringe, we generated a bulk flow rate of 3.33 μL min^{-1} in the channel. By activating the acoustofluidic chip with a 24.5 V and 4.8 kHz signal, we were able to trap 20 μm particles along the sharp edge surface, while the 2.5 μm particles continued to be pumped through the channel (Fig. 5d and Video S2 in the ESI†). This is consistent with the acoustic radiation force and streaming equations used to describe bubble-based systems, where the acoustic radiation force scales with the radius of the particles cubed. Thus, the larger particles experience significantly larger radiation force and are pulled towards the oscillating sharp-edges while the smaller particles do not become trapped. Turning off the acoustic signal releases the larger particles and they resume their path towards the channel outlet (Fig. 5e). Similar to other streaming based particle traps, there is a limit to the number of particles that can be held within the trap before it starts to lose efficiency.[34] The limit for the entire system could be increased by increasing the length of the channel, as well as the number of traps for particles to be captured in. A separation system could then be operated in a pulsatile manner, where the particles of interest flow freely through to be collected as a purified sample. Once the traps reach capacity, the user would turn off the acoustic signal and collect the next portion as waste before reactivating the acoustic signal and resuming collection. Alternatively, if the larger particles are desirable, then this system could be used to concentrate many particles into a smaller volume. In combination with the portable power supply and syringe pump, this system could be used to isolate particles of interest from biological samples for POC diagnosis.[21,35]

As an additional example of the expandable nature of the Arduino system, we integrated a camera and lens system to enable portable microscopic imaging. To achieve this, we combined a 5 MP Arduino compatible camera (0V5642, Arducam) with a low-cost microscope lens system designed for use with cell phones (CML-60X-100X-BL-01, Efanr®). We tested the imaging capabilities using the 1951 USAF Resolution test (Fig. 6a), which contains successively smaller bars to identify the resolution limit of an optical platform; the system has a group/element system that is used to identify the approximate resolution of a system. The cut-out provided in Fig. 6a shows that the smallest bars discernible by the system are located in element 2 of group 7, which suggests an optical resolution of 3.48 μm. We then compared the image quality of the platform side-by-side with our benchtop microscope (comparison provided in Fig. 6b). The pillars shown in the images are 100 μm wide and located at the end of the sputum liquefaction chip as a filtration system for undesirable particles; although the edges in the photo taken by the Arduino platform are not as crisp, the image still provides a detailed view, even at these microchannel sized resolutions. Lastly, we used the portable platform to image a *C. elegans* within the rotation chamber (Fig. 6c). The quality of the image is not as high as those provided in Fig. 3, but the oocytes within the worm are still discernible. We also note that with the low-cost microscope lens we used, there is some distortion near the edges which blurs the head and tail. This issue could be remedied with higher quality components. Obviously, these higher quality components would come with an increased cost; it is up to the future developer to identify their desired image quality and price-point to determine the optical components that work best for their needs. Additionally, integrating excitation and emissions filters into the lens system would enable fluorescent imaging of the worms, potentially providing a

Author Manuscript Author Manuscript Author Manuscript Author Manuscript

comprehensive and portable platform for worm analysis. In total, the image testing conducted serves to demonstrate the feasibility of creating a completely portable acoustofluidic platform. Integrating portable data storage into the system would enable POC data collection, where it could be analyzed immediately, or stored for analysis where resources are available.

Conclusions

The Arduino based platform presented in this work serves to replace the complex external equipment typically associated with acoustofluidic device operation. Throughout the design of this Arduino based open source system, we demonstrated how the system could be modified for use in settings where power is available from outlets, or where battery power is required. Additionally, we were able to achieve, for the first time, highly precise rotation and manipulation of cells and microorganisms, as well as the control of a chip which has previously been utilized for the liquefaction of sputum samples, and even separation of particles based on size, all in a portable fashion. The expandability of the platform was also illustrated through the addition of a portable syringe pump, as well as portable microscope functionality. These applications have great potential in transforming biomedical research, and personal medicine in lower resource settings, paving the way for future progress and discovery. The ability to expand the open source acoustofluidic system with any number of commercially available parts means that researchers can tailor their unique acoustofluidic system to meet their specific needs. Additionally, the open source nature of the platform means that researchers will have access to the hardware and software needed to successfully modify their own platforms. With further modification, it is possible to expand the frequency range of the technology to much higher values; this provides researchers with the opportunity to implement additional acoustofluidic technologies at the POC, well beyond the scope of devices presented in this work. Altogether, the open source acoustofluidic system designed in this work presents many unique and influential opportunities for the acoustofluidics and microfluidics communities. It is our hope that this system can serve as a roadmap for how research groups in other fields can begin to adapt their technologies for use by a broader community. We also hope that this work can serve to demonstrate the simplistic nature of acoustofluidic technologies and that the open source nature of the materials enables a wider audience to incorporate these solutions into their work.

Supplementary Material

Refer to Web version on PubMed Central for supplementary material.

Acknowledgements

We acknowledge support from the National Institutes of Health (R01 GM132603, R01GM127714, R43 OD024963, P42ES010356, and F32 ES027306 (JHH)), and the United States Army Medical Research Acquisition Activity (W81XWH-18-1-0242).

References

1. Gervais L, De Rooij N and Delamarche E, Adv. Mater, 2011, 23, H151–H176. [PubMed: 21567479]
2. Chin CD, Linder V and Sia SK, Lab Chip, 2012, 12, 2118–2134. [PubMed: 22344520]

Author Manuscript Author Manuscript Author Manuscript Author Manuscript

3. Sia SK and Kricka LJ, Lab Chip, 2008, 8, 1982. [PubMed: 19023459]
4. Lillehoj PB, Huang MC, Truong N and Ho CM, Lab Chip, 2013, 13, 2950–2955. [PubMed: 23689554]
5. Liu C, Geva E, Mauk M, Qiu X, Abrams WR, Malamud D, Curtis K, Owen SM and Bau HH, Analyst, 2011, 136, 2069–2076. [PubMed: 21455542]
6. Lillehoj PB, Wei F and Ho CM, Lab Chip, 2010, 10, 2265–2270. [PubMed: 20596556]
7. Ahmed H, Destgeer G, Park J, Jung JH, Ahmad R, Park K and Sung HJ, Anal. Chem, 2017, 89, 13575–13581. [PubMed: 29156880]
8. Huang P-H, Yang S, Zhang P, Huang TJ, Bachman H, Fu H and Zhao S, Lab Chip, 2018, 18, 433–441. [PubMed: 29302660]
9. Wu M, Ouyang Y, Wang Z, Zhang R, Huang P-H, Chen C, Li H, Li P, Quinn D, Dao M, Suresh S, Sadovsky Y and Huang TJ, Proc. Natl. Acad. Sci. U. S. A, 2017, 114, 10584–10589. [PubMed: 28923936]
10. Zhang SP, Lata J, Chen C, Mai J, Guo F, Tian Z, Ren L, Mao Z, Huang P-H, Li P, Yang S and Huang TJ, Nat. Commun, 2018, 9, 2928. [PubMed: 30050088]
11. Li P and Huang TJ, Anal. Chem, 2019, 91, 757–767. [PubMed: 30561981]
12. Ozcelik A, Rufo J, Guo F, Gu Y, Li P, Lata J and Huang TJ, Nat. Methods, 2018, 15, 1021–1028. [PubMed: 30478321]
13. Guo F, Li P, French JB, Mao Z, Zhao H, Li S, Nama N, Fick JR, Benkovic SJ and Huang TJ, Proc. Natl. Acad. Sci. U. S. A, 2015, 112, 43–48. [PubMed: 25535339]
14. Leibacher I, Reichert P and Dual J, Lab Chip, 2015, 15, 2896–2905. [PubMed: 26037897]
15. Whitehill JD, Gralinski I, Joiner D and Neild A, J. Nanopart. Res, 2012, 14, 1223.
16. Mao Z, Li P, Wu M, Bachman H, Mesyngier N, Guo X, Liu S, Costanzo F and Huang TJ, ACS Nano, 2017, 11, 603–612. [PubMed: 28068078]
17. Huang P-H, Ren L, Nama N, Li S, Li P, Yao X, Cuento RA, Wei C-H, Chen Y, Xie Y, Nawaz AA, Alevy YG, Holtzman MJ, McCoy JP, Levine SJ and Huang TJ, Lab Chip, 2015, 15, 3125–3131. [PubMed: 26082346]
18. Orbay S, Ozcelik A, Lata J, Kaynak M, Wu M and Huang TJ, J. Micromech. Microeng, 2016, 27, 015008. [PubMed: 31588165]
19. Huang P-H, Xie Y, Ahmed D, Rufo J, Nama N, Chen Y, Chan CY and Huang TJ, Lab Chip, 2013, 13, 3847–3852. [PubMed: 23896797]
20. Huang P-H, Nama N, Mao Z, Li P, Rufo J, Chen Y, Xie Y, Wei C-H, Wang L and Huang TJ, Lab Chip, 2014, 14, 4319–4323. [PubMed: 25188786]
21. Petersson F, Åberg L, Swärd-Nilsson AM and Laurell T, Anal. Chem, 2007, 79, 5117–5123. [PubMed: 17569501]
22. Ai Y, Sanders CK and Marrone BL, Anal. Chem, 2013, 85, 9126–9134. [PubMed: 23968497]
23. Shi J, Ahmed D, Mao X, Lin S-CS, Lawit A and Huang TJ, Lab Chip, 2009, 9, 2890–2895. [PubMed: 19789740]
24. Ahmed D, Ozcelik A, Bojanala N, Nama N, Upadhyay A, Chen Y, Hanna-Rose W and Huang TJ, Nat. Commun, 2016, 7, 11085. [PubMed: 27004764]
25. Carrilho E, Martinez AW and Whitesides GM, Anal. Chem, 2009, 81, 7091–7095. [PubMed: 20337388]
26. Lu Y, Shi W, Qin J and Lin B, Anal. Chem, 2010, 82, 329–335. [PubMed: 20000582]
27. Gervais L, Hitzbleck M and Delamarche E, Biosens. Bioelectron, 2011, 27, 64–70. [PubMed: 21752632]
28. Hitzbleck M, Gervais L and Delamarche E, Lab Chip, 2011, 11, 2680–2685. [PubMed: 21674120]
29. Gervais L and Delamarche E, Lab Chip, 2009, 9, 3330–3337. [PubMed: 19904397]
30. Pan S, Deen MJ, Dong S, Ghosh R, Alam AU, Jin H and Qin Y, J. Chem. Educ, 2017, 95, 326–330.
31. Zhang C, Wijnen B and Pearce JM, J. Lab. Autom, 2016, 21, 517–525. [PubMed: 26763293]
32. Lake JR, Heyde KC and Ruder WC, PLoS One, 2017, 12, e0175089. [PubMed: 28369134]

Author Manuscript Author Manuscript Author Manuscript Author Manuscript

33. Ozcelik A, Nama N, Huang PH, Kaynak M, McReynolds MR, Hanna-Rose W and Huang TJ, Small, 2016, 12, 5120–5125. [PubMed: 27515787]
34. Patel MV, Nanayakkara IA, Simon MG and Lee AP, Lab Chip, 2014, 14, 3860–3872. [PubMed: 25124727]
35. Hajko V, Energy Stud. Rev, 2013, 20, 1–23.
36. Hashmi A, Yu G, Reilly-Collette M, Heiman G and Xu J, Lab Chip, 2012, 12, 4216–4227. [PubMed: 22864283]
37. Miller DL, J. Acoust. Soc. Am, 2005, 84, 1378–1387.

Author Manuscript
Author Manuscript
Author Manuscript
Author Manuscript

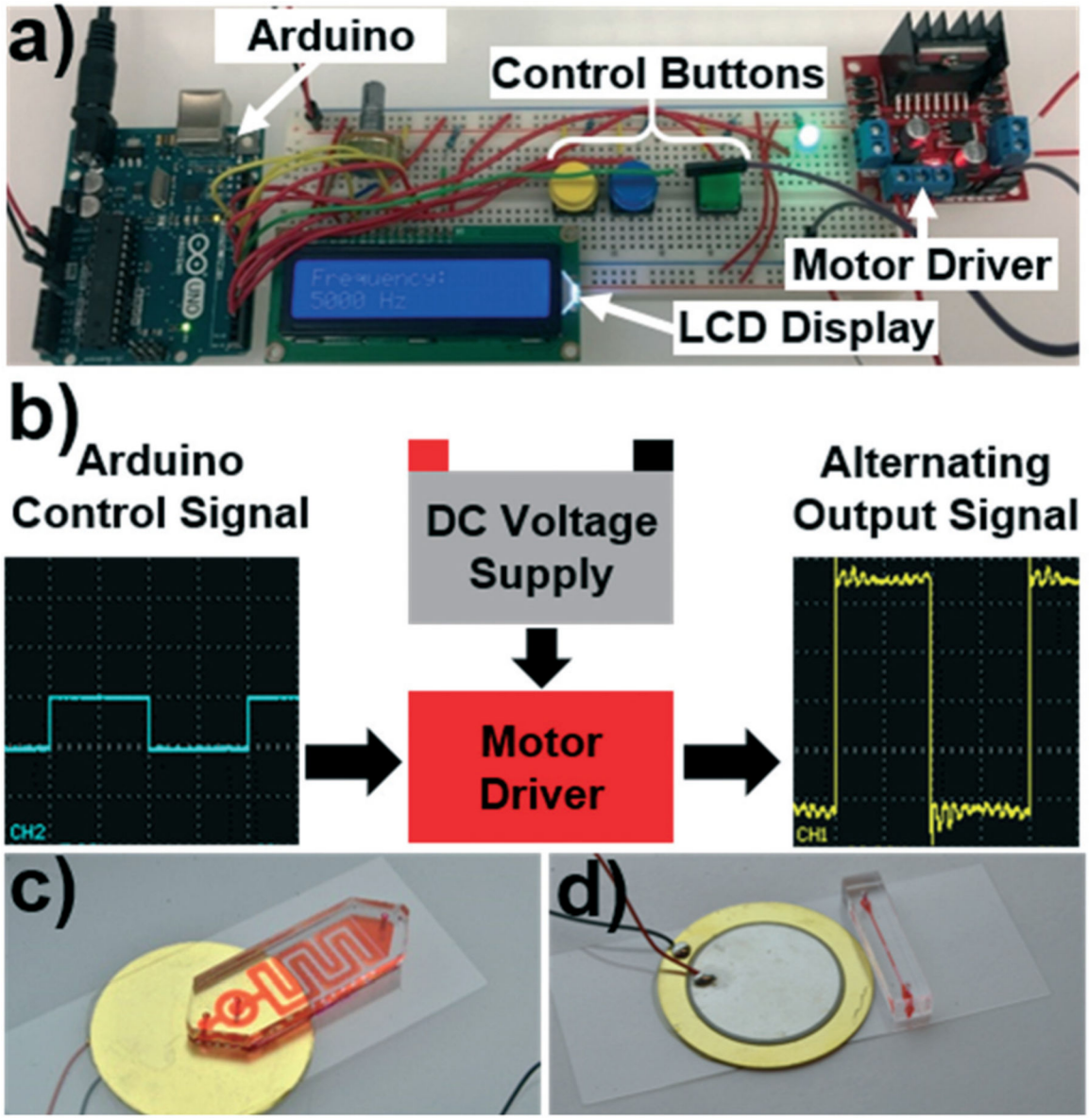

Fig. 1.

a) Photo of the open source control platform designed around the Arduino prototyping board. b) Schematic detailing the working mechanism of the control platform. The Arduino provides an alternating signal that controls a motor driver that gates a high voltage source. As the motor driver opens and closes the circuit, the high voltage signal is passed to the transducer in the requisite alternating pattern. Photos of the c) sharp edge based and d) bubble based acoustofluidic devices, which are two of the acoustofluidic devices that are compatible with the platform.

Author Manuscript Author Manuscript Author Manuscript Author Manuscript

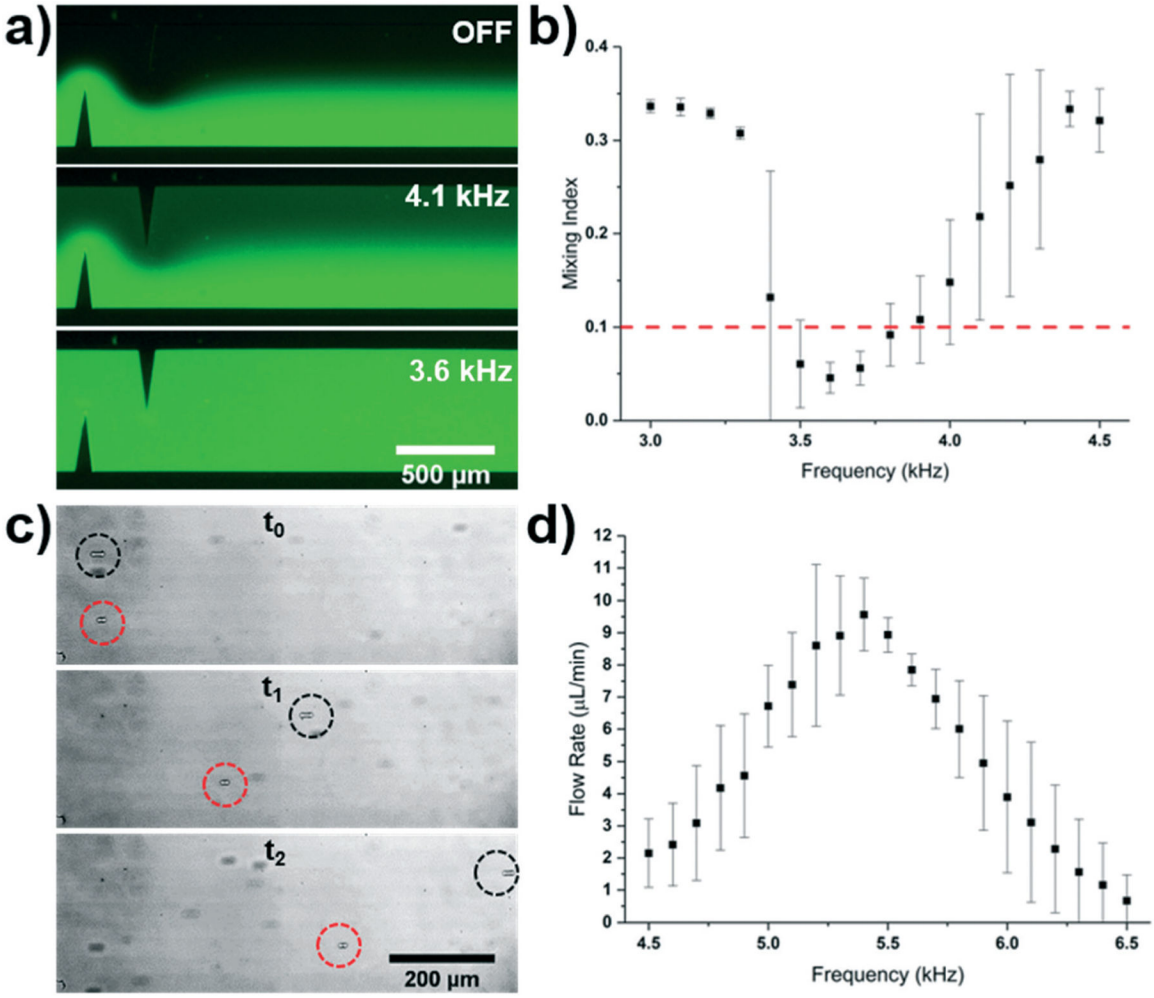

Fig. 2.

a) Fluorescent mixing achieved when applying varying frequencies to the sharp-edge based acoustofluidic device. b) Plot of the mixing index versus frequency for the sharp-edge based acoustofluidic mixer controlled by the Arduino system. A 35 V signal and a 10 µL min^{-1} total flow rate was used for the mixing experiment. c) Overlaid particle tracing when the sharp-edge based acoustofluidic micropump was operated at two different frequencies. Both particles were pumped with a 30 V signal; the black and red circles track particles pumped using a 5.4 kHz and 6.1 kHz signal, respectively. Time between t_0 and t_2 was 288 ms. d) Plot of the pumping flow rate versus frequency for the sharp-edge based acoustofluidic micropump controlled by the wall-powered Arduino system. A 30 V signal was applied to the sharp edge pump.

Author Manuscript Author Manuscript Author Manuscript Author Manuscript

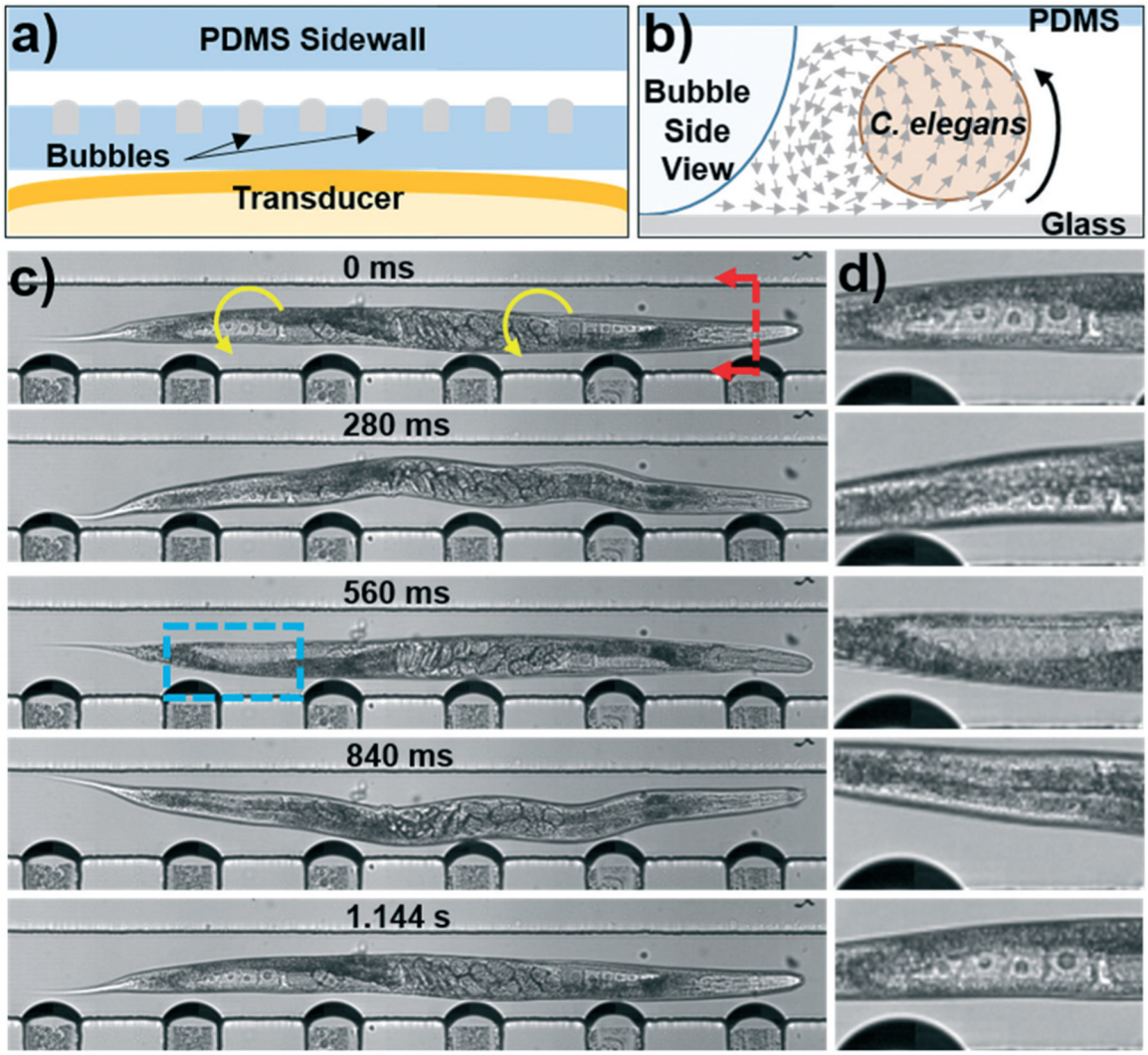

Fig. 3.

a) Schematic of the bubble-based acoustofluidic device. b) Schematic of out-of-plane streaming used to rotate *C. elegans*. c) Photos taken throughout the rotation of a *C. elegans*. A 20 V, 19.1 kHz signal was applied to the transducer to induce bubble vibration and *C. elegans* rotation. The blue box indicates the location of the (d) close-up of the proximal distal gonad provided on the right hand side of each photo. Oocytes can be seen clearly as they rotate into and out of the focal plane of the camera.

Author Manuscript Author Manuscript Author Manuscript Author Manuscript

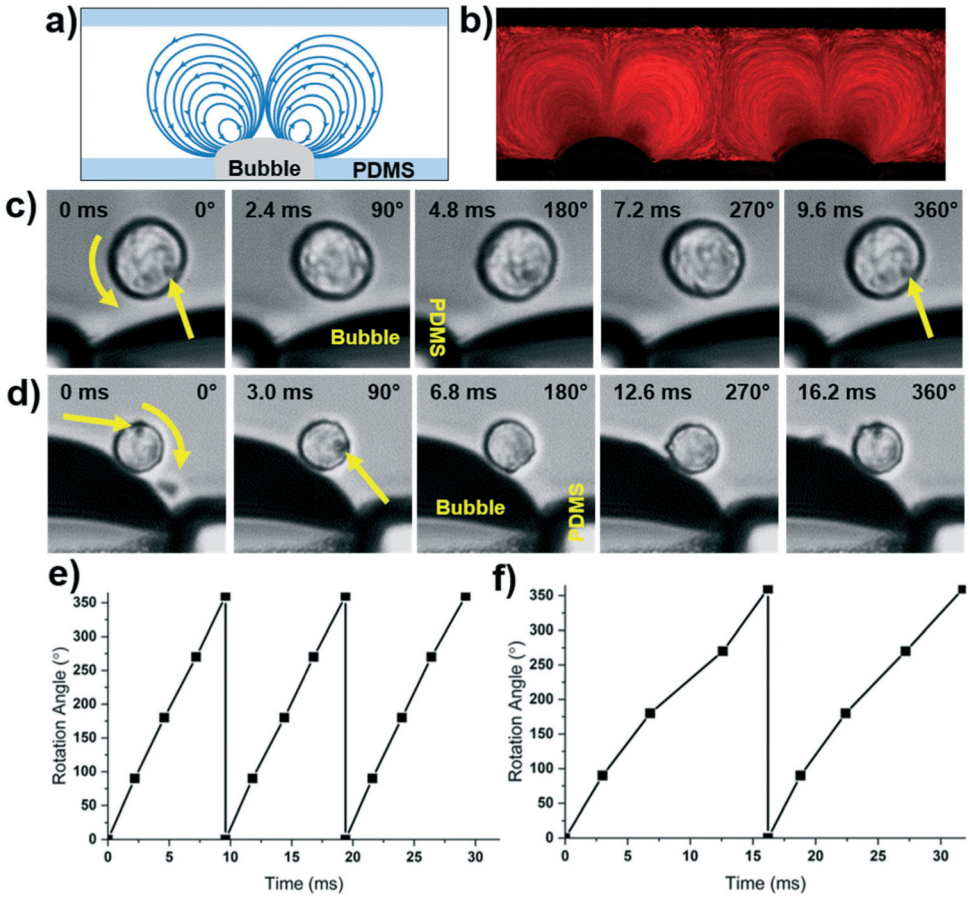

Fig. 4.

a) Schematic and b) particle tracing of in-plane rotation using the bubble-based acoustofluidic rotation device and a battery powered Arduino control platform. c) Counterclockwise and d) clockwise bubble-based rotation of HeLa cells using a battery powered Arduino system. The top and bottom cells were rotated via excitation by a 25 V, 20.9, and 21.8 kHz signal, respectively. e) Plot of counterclockwise and f) clockwise rotation angle of cells *versus* time using the bubble-based acoustofluidic device.

Author Manuscript Author Manuscript Author Manuscript Author Manuscript

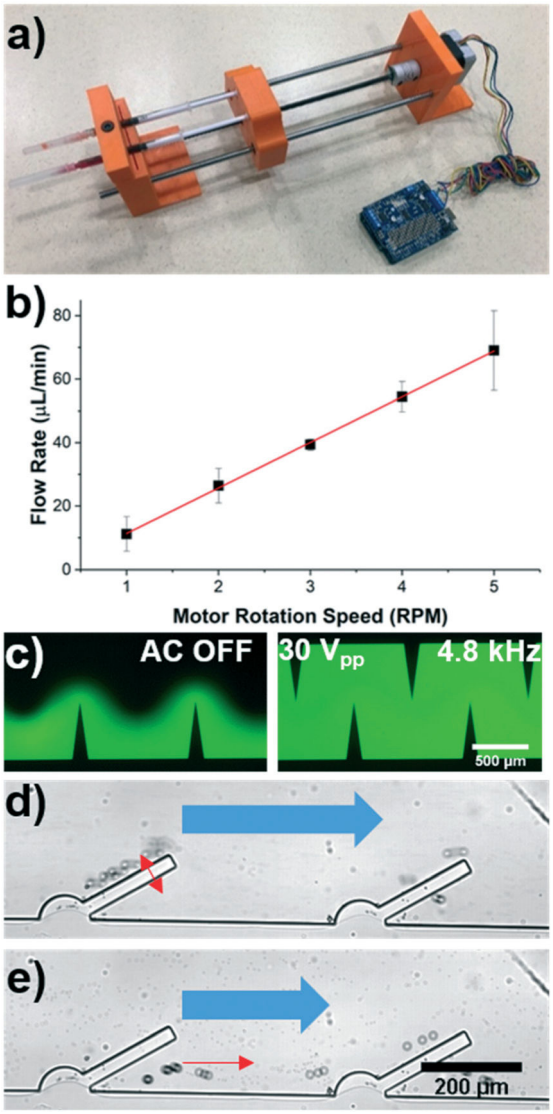

Fig. 5.

a) Photo of the portable syringe pump that is controlled by an Arduino board. b) Flow rate characterization at different rotational speeds of the motor; a linear fit is included with the data (r^2 = 0.9995). c) Fluorescent images of mixing in the sputum liquefaction chip with the acoustic signal OFF (left) and ON (right). The acoustic signal was 30 V_{pp} and 4.8 kHz, with a total flow rate in the channel of 79 μL min^{-1}. d) Trapping and e) release of 20 μm particles using a sharp-edge acoustofluidic device. 2.5 μm particles continue to flow through the channel even when the acoustic signal is on. Red arrows indicate large particle motion, and the bulk flow and small particle movement is marked by the blue arrows.

Author Manuscript Author Manuscript Author Manuscript Author Manuscript

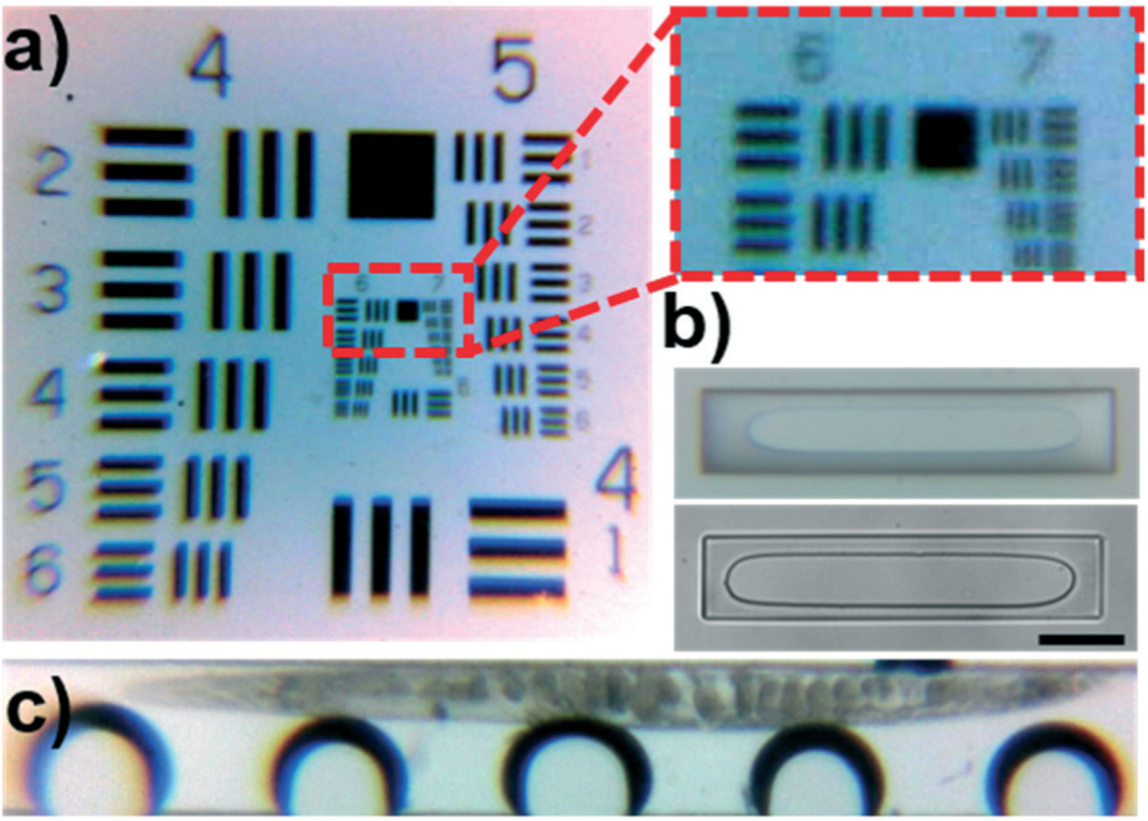

Fig. 6.

a) Photo of a 1951 USAF resolution target and expanded view of the smallest discernible section. The visible lines in the second element of the seventh group suggests a resolution limit around 3.5 μm. b) Comparative photos of 100 μm wide pillars imaged using the Arduino (top) and benchtop microscope with a 10x objective (bottom). Scale bar is 100 μm. c) Image taken of a *C. elegans* in the rotation device using the Arduino microscope.

Author Manuscript Author Manuscript Author Manuscript Author Manuscript

Table 1

Acoustofluidic device control requirements and open source equivalents used to achieve this functionality. Parameters achieved by the portable system are included in the right side of the table

Acoustofluidic system operation		
Traditional device needed	**Open source equivalent**	**Parameter achieved with open source system**
Function generator	Arduino Uno board	30 Hz-65 kHz
Amplifier	DC power and motor driver board	12–50 V
Syringe pump	3D printed syringe pump	>3.3 μL min^{-1}
Microscope	Arduino compatible camera	>3.5 μm resolution

Lab Chip. Author manuscript; available in PMC 2020 January 21.